Biogeosciences, 6, 2589–2598, 2009
www.biogeosciences.net/6/2589/2009/

Biogeosciences

Coupling of surface pCO_2 and dissolved oxygen in the northern South China Sea: impacts of contrasting coastal processes

W. D. Zhai[1], **M. Dai**[1], **and W.-J. Cai**[2]

[1]State Key Laboratory of Marine Environmental Science, Xiamen University, Xiamen 361005, China
[2]Department of Marine Sciences, University of Georgia, Athens, GA 30602–3636, USA

Received: 8 June 2009 – Published in Biogeosciences Discuss.: 30 June 2009
Revised: 25 September 2009 – Accepted: 29 September 2009 – Published: 16 November 2009

Abstract. We examined the relationship between CO_2 partial pressure (pCO_2) and dissolved oxygen (DO) based on a cruise conducted in July 2004 to the northern South China Sea (111°–118° E 18°–23° N), spanning from estuarine plume, coastal upwelling and deep basin areas. Distinct relationships between pCO_2 and DO saturation were identified in different regimes. In coastal upwelling areas and the Pearl River estuary, biological drawdown of pCO_2 and production of O_2 were simultaneously observed. The two properties were coupled with each other primarily via photosynthesis and respiration. The stoichiometric relationship of the two properties however, was quite different in these two environments due to different values of the Revelle factor. In the offshore areas, apart from the estuary and upwelling, the dynamics of pCO_2 and DO were mainly influenced by air-sea exchange during water mixing. Given the fact that air-sea re-equilibration of O_2 is much faster than that of CO_2, the observed pCO_2-DO relationship deviated from that of the theoretical prediction based on the Redfield relationship in the offshore areas. Although this study is subject to the limited temporal and spatial coverage of sampling, we have demonstrated a simple procedure to evaluate the community metabolic status based on a combination of high-resolution surface pCO_2 and DO measurements, which may have applicability in many coastal systems with a large gradient of changes in their physical and biogeochemical conditions.

1 Introduction

The production of organic carbon leads to drawdown of CO_2 partial pressure (pCO_2) and increases in dissolved oxygen (DO), while respiration/remineralization is associated with CO_2 release and DO consumption. It is therefore reasonable to expect a correlation between pCO_2 and DO in the surface ocean. Such a correlation has been shown to have implications for upper ocean metabolic status, i.e. primary production/respiration and their history (DeGrandpre et al., 1997, 1998; Álvarez et al., 2002; Gago et al., 2003; Carrillo et al., 2004; Kuss et al., 2006; Körtzinger et al., 2008). Indeed, many studies have used simultaneous measurements of DO and CO_2 in seawater to investigate the effects of metabolic processes on the oceanic CO_2 dynamics (Borges and Frankignoulle, 2001; Guéguen and Tortell, 2008; Zhai and Dai, 2009). However, it is important to recognize that sea surface pCO_2 is buffered by the marine carbonate system, while DO is not associated with any buffer system. Therefore the relationship between the pCO_2 and DO variation in the euphotic zone may differ between different biogeochemical settings (DeGrandpre et al., 1997, 1998), thereby having different implications in terms of constraining net metabolic status of the system. The coastal system, due to its large gradients in physical properties and biogeochemistry, may be particularly prone to such variability. Thus far, there have only been a few reports attempting to elucidate such relationships in the context of ecosystem metabolic balance based on high spatial-resolution measurements of CO_2 and O_2 (e.g. Carrillo et al., 2004).

In the summer of 2004, we conducted underway measurements of surface pCO_2 and DO in the northern South China Sea, surveying estuarine plume, coastal upwelling and deep basin areas (Fig. 1). This dataset allowed for a close examination of how the relationship between pCO_2 and DO might vary between contrasting coastal regimes, such as open offshelf regions and near-shore coastal areas influenced by either an estuarine plume and/or coastal upwelling. We discussed how such contrast and variability might affect the interpreation of the pCO_2 and DO observation in terms of constraining net metabolic status. Based upon a limited data set though, this study sought to demonstrate a simple procedure

Correspondence to: M. Dai
(mdai@xmu.edu.cn)

Published by Copernicus Publications on behalf of the European Geosciences Union.

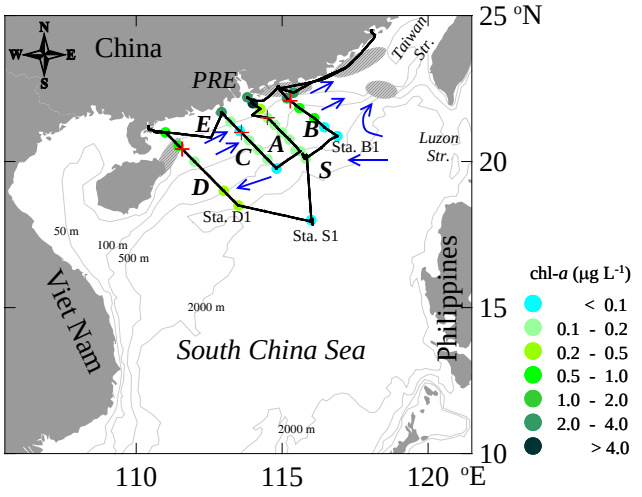

Fig. 1. Map of the northern South China Sea showing the cruise track and surveying transects (A, B, C, D, E and S). "+" symbols designate locations where we used to divide the shelf into nearshore and offshore areas in this study. Stations B1, D1 and S1 are also shown. Shadowed ellipses sketch typical summer upwelling locations based on Wu and Li (2003) and Jing et al. (2009). Blue arrows sketch major currents in summer based on Hu et al. (2000), including the seasonal northeastward coastal current (in summer) along the 50 m isobath, the year-around northeastward South China Sea Warm Current along the 100 m isobath, and a strong year-around westward South China Sea Branch of Kuroshio. Discretely sampling data of surface chlorophyll-*a* (chl-*a*) concentrations were from Huang et al. (2008).

to evaluate the community metabolic status based on a combination of high-resolution surface pCO_2 and DO measurements, which may have applicability in many coastal systems with a large gradient of changes in their physical and biogeochemical conditions.

2 Materials and methods

2.1 Study area and survey transects

The South China Sea (SCS) is the world's largest marginal sea, located at low (tropical/subtropical) latitudes. While its maximum depth exceeds 5000 m, it has extensive shelf and slope systems towards the northwestern and southern boundaries, with a mean depth of only 1350 m (Wong et al., 2007). The northern shelf and slope region (referred to as the northern SCS hereafter, ~200 km wide) is oligotrophic, hence has low-production (Wong et al., 2007; Chen and Chen, 2006) and serves as a net source of atmospheric CO_2, especially in summer (Zhai et al., 2005a). This is in contrast to several significant CO_2-sink cases in mid-latitude continental shelf systems (Cai and Dai, 2004; Borges et al., 2005; Cai et al., 2006; Chen and Borges, 2009).

The nearshore waters of the northern SCS are quite different from the oligotrophic offshore regions. Fed by the Pearl River, a major world river located in southern China, the productive estuarine plume may extend southeastward to up to a few hundred kilometers from the estuary mouth in flooding seasons (Dai et al., 2008; Gan et al., 2009). In addition to the estuarine plume, the northern SCS is also influenced by seasonal upwelling along the Chinese coast (Fig. 1; Han, 1998; Wu and Li, 2003; Gan et al., 2009; Jing et al., 2009). Both processes peak in summer as a result of the prevailing, rain-bearing southwest monsoon from late May to September (Han, 1998), and both contribute a significant amount of new nutrients to the coastal waters, inducing dramatic changes of surface pCO_2 and DO through enhanced primary productivity (e.g. Dai et al., 2008). The contrast between productive nearshore and oligotrophic offshore areas in the northern SCS was clearly shown by the chlorophyll *a* (chl-*a*) dataset (Fig. 1; Huang et al., 2008), which was determined by fluorescence analysis of discrete filtered samples, and the standard material was taken by HPLC.

Our cruise was conducted on 6–23 July 2004 on board the R/V Yanping II. During this cruise, we performed underway measurements of temperature, salinity, DO and pCO_2 along four shelf-crossing transects (Fig. 1, sequentially marked as B, D, C and A from the cruise beginning to the end) and an alongshore transect (E). Transect A covers the Pearl River estuary (114°00′ E 22°00′ N, PRE hereafter) southwest to the Dongsha Islands (115°48′ E 20°10′ N). The final leg formed the transect between station B1 (116°54′ E 20°52′ N) and the deep basin station (Station S1, 116°00′ E 18°00′ N), named Transect S (Fig. 1). In this study, nearshore areas and coastal waters were separated from the deeper offshore region as Fig. 1.

2.2 Sampling, analyses and data processing

During the cruise, surface water (at a depth of 1–2 m) was continuously pumped from a side intake using an underway pumping system similar to that previously described in Zhai et al. (2005b). Sea surface temperature (SST) and salinity were measured continuously using a SEACAT thermosalinograph system (CTD, SBE21, Sea-Bird Co.) with an inlet temperature sensor (SBE 38 remote sensor, with a precision of 0.001°C, measuring ahead of the water pump). Data were recorded every 6 s and averaged to 1 min. This underway CTD system was calibrated just prior to the cruise.

Surface water pCO_2 was determined using an underway system with a continuous flow and cylinder-type equilibrator (9 cm in diameter and 20 cm long) that is filled with plastic balls and enclosed with ~100 mL of the headspace (Zhai et al., 2005b). Water flow rate was set to about 4 L min^{-1}. A Yellow Springs Instrument meter (YSI6600) was used to continuously measure temperature (with a precision of 0.01°C) in the equilibrator. Based on inter-calibration testing, we estimated that all onboard temperature sensors are

consistent with each other within 0.1°C. After the equilibrator and dehydration, the CO_2 mole fraction in dry air (xCO_2) was detected continuously using a Li-Cor NDIR spectrometer (Li-7000). Data were recorded every 5 s and averaged to 1 min. The NDIR spectrometer was calibrated regularly against 4 CO_2 gas standards. xCO_2 of the standards ranged from 138 to 967 μmol mol^{-1}. pCO_2 was converted from corrected xCO_2 based on barometric pressure measured by the Li-7000 detector or air pressure along the transect. The latter were collected every minute with an onboard weather station at 10 m height above the sea surface. Comparison between the two air pressure datasets revealed consistency at a relative error level of 0.1% (i.e. 1 hPa). The Weiss and Price (1980) saturated water vapor pressure and the Takahashi et al. (1993) temperature effect coefficient of 4.23%°C^{-1} were used to calculate the in situ pCO_2. The temperature difference between the equilibrator and the sea surface (i.e. the inlet temperature) was 0.21–0.29°C. The overall uncertainty of the xCO_2 measurements and pCO_2 data processing was <1%, as constrained by our standard gases (Zhai et al., 2005a, b).

Air pCO_2 was determined during the first 5 days, every 1–3 h in daytime and every 4 h at nighttime, using the same NDIR spectrometer and dehydration system. The bow intake from which atmospheric air was pumped was installed at ~6 m above the water surface to avoid contamination from the ship. The air pCO_2 data were corrected to 100% humidity at SST and sea surface salinity.

Surface DO was continuously measured using a pulsed polarographic electrode incorporated with the above-mentioned YSI meter. Data were recorded every 12 s and averaged to 1 min. The DO sensor was pre-calibrated against air saturated pure water and post-calibrated by simultaneous discrete Winkler DO data. These discrete samples were either collected via a side vent of our pumping system or obtained using 2.5-L Go-Flo bottles during general station work. DO concentration at equilibrium with the atmosphere was calculated from the Benson and Krause (1984) equation and local air pressure.

According to Broecker and Peng (1982) and Stigebrandt (1991), air bubbles in the surface layer, created by breaking surface waves, can result in a DO super-saturation of 2.5% in open sea areas. In this study, we used the fixed 2.5% super-saturation as the effective DO saturation level considering the bubble effect, which should be reasonable based on the range of our field-observed surface DO (103% −107%, Fig. 2f), the trend of which was consistent with the chl-*a* (from <0.1 to 0.2 μg L^{-1}, Fig. 1) although the area is generally very low in biological production. Therefore we defined excess oxygen (EO_2 hereafter) as Eq. (1) to reflect evasion or invasion of atmospheric O_2:

$$EO_2 = [O_2] - 1.025 \times [O_2]_{eq} \quad (1)$$

where $[O_2]$ is the field-measured DO concentration; $[O_2]_{eq}$ the DO concentration at equilibrium with the atmosphere, calculated from the Benson and Krause (1984) equation and local air pressure. The negative EO_2 suggests an O_2 deficit while a positive value means O_2 emission from water to the atmosphere. Note that the bubble effect on surface DO might be subject to variations given the regional heterogeneity in terms of surface wave field.

3 Results

3.1 Data overview

During the cruise, two high salinity water masses were identified (Figs. 2, 3). One was a typical SCS surface water with salinity of 33.7–34.5 and SST of 28–31°C. All of the offshore areas of the four cross-shelf transects and the eastern area of transect E are dominated by this water mass (Fig. 2). In this water mass, surface DO was slightly oversaturated (103%–110%), while pCO_2 ranged 370–400 μatm. Both were consistent with the generally oligotrophic and low productive feature of the SCS surface water (Zhai et al., 2005a; Chen and Chen, 2006; Tseng et al., 2007).

Another high salinity water mass was characterized by low temperatures of 25.5–26.5°C (Figs. 2, 3), suggesting the influence of subsurface water upwelling. This water mass was limited to the nearshore area of Transect B and to the west side of Transect E. The nearshore area of Transect D was also influenced by the same low temperature water as observed in Transect E (Fig. 2). These two upwelling-influenced coastal areas have been well defined by both field measurements (Wu and Li, 2003) and numerical modeling (Jing et al., 2009). The upwelling may support higher productivity due to new nutrient input from depth. Thus, moderate to high chl-*a* levels were observed in these areas, especially in the nearshore areas of Transect B (Fig. 1). Significantly oversaturated DO concentrations of 120%–138% associated with the low temperatures were also observed in these areas, especially in the nearshore areas of Transect D (Fig. 2d). However, pCO_2 varied in a large range between 280 and 440 μatm (Fig. 2), of which the highest pCO_2 of >400 μatm was observed at the west side of Transect E (Fig. 2e).

The low salinity water (S<33) could also be clustered into two groups (Fig. 3). One had a similar temperature (~28.5°C) to the PRE water (27–28°C, Fig. 2a), situated in nearshore areas of Transects A, B, C and E (Fig. 2). Another low-salinity water mass, located in offshore water along Transect B had fairly high temperatures (30.5–31.0°C) (Fig. 2b). The latter water mass had relatively low chl-*a* (Fig. 1) and nearly air-equilibrated DO (Fig. 2b) compared to the upwelling-influenced, nearshore area. This offshore, low-salinity water was likely to be of estuarine origin from the PRE plume, which is typical in this region in summer as reported by Gan et al. (2009). Both May and July were major rainy months in 2004 within the drainage basin of the Pearl River and heavy rainfall of 100–300 mm occurred during 10–12 May 2004 (China MWR-BH, 2005). Therefore, the patchy offshore low-salinity water in Transect B may

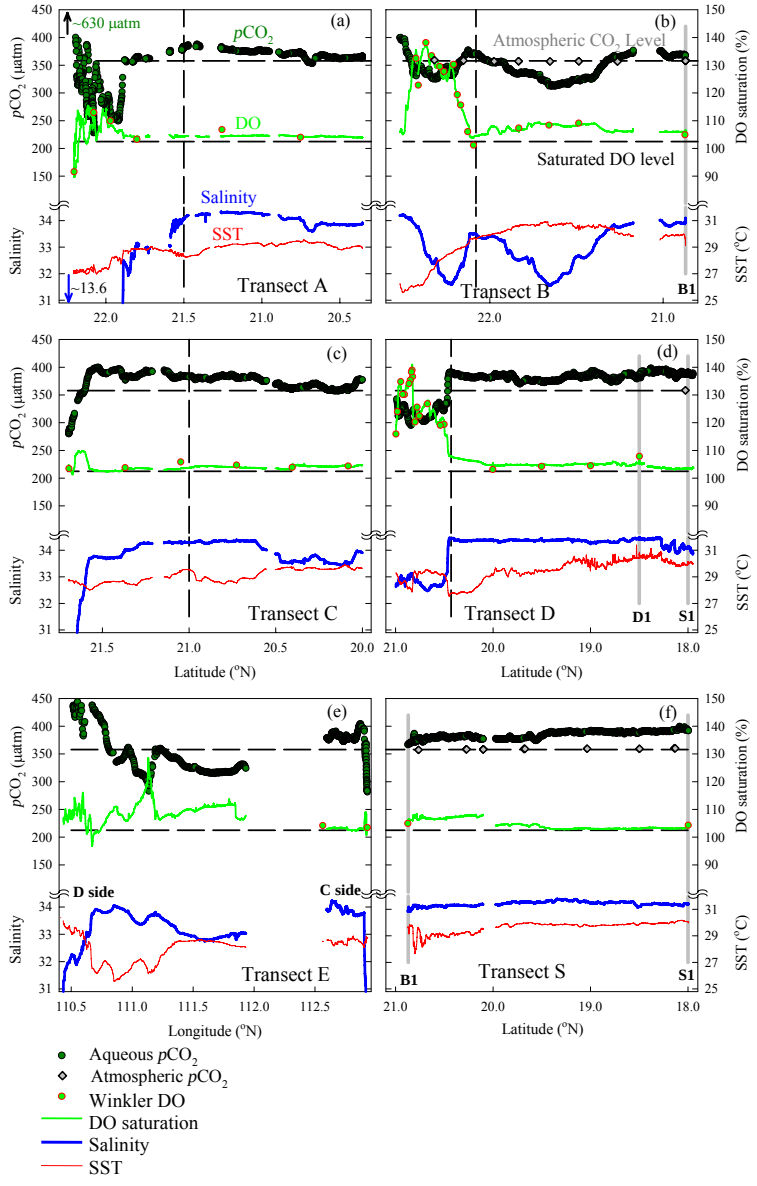

Fig. 2. Distribution of surface T, S, pCO_2 and DO along surveying transects. Note that Panels **(a)**–**(d)** and **(f)** are presented from the coast (north) to the deep basin (south). Panel **(e)** is presented from Transect D side (west) to Transect C side (east). A high pCO_2 of 630 μatm and a low salinity of 13.6 in the Pearl River estuary, as extended from Transect A were marked in panel (a). The vertical dashed lines in panels (a)–(d) show the locations where we used to divide the shelf into nearshore and offshore areas in this study, referring to Fig. 1. The vertical grey solid lines in panels **(b)**, (d) and (f) show Stations B1, S1 and D1, referring to Fig. 1. The horizontal dashed lines in each panel show atmospheric CO_2 level (upper) and saturated DO level (lower).

have originated from the PRE after this heavy rain-induced flood, followed by partial mixing with typical northern SCS surface water. Based on weather report and reports given in a cruise just prior to ours, i.e. Chen and Chen (2006), we concluded that it is unlikely that a local rainfall could be the cause of the low salinity.

Both of the nearshore and offshore low-salinity water masses had understaturated pCO_2 of 310–350 μatm (Fig. 2), while DO varied from the highly over-saturated level of 138% nearshore to the only slightly over-saturated level of 103%–110% offshore (Fig. 2b). Note that in the PRE and the adjacent coastal waters (salinity <25), although chl-*a* was as high as 3–5 μg L^{-1} (Fig. 1; Huang et al., 2008), indicating the significant primary production, surface DO saturation was no higher than 115% (Fig. 2a).

Figure 4 geographically shows the distributions of field-measured sea surface salinity, temperature, pCO_2 and DO saturation in July 2004 in the northern SCS under study.

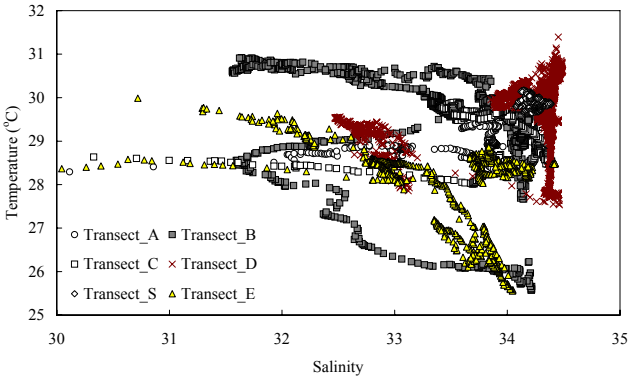

Fig. 3. Surface T-S diagram for salinity >30. Note that in the PRE and the adjacent coastal waters, salinity was <25 along with a temperature of 27–29°C (Fig. 2a).

3.2 Relationship between pCO_2 and DO

In the PRE and nearshore region of Transect A, pCO_2 and DO saturation had a significant negative correlation (Fig. 5a). Based on our previous studies, the freshwater end of the PRE is characterized by high pCO_2 and low DO (Zhai et al., 2005b), while the estuarine plume has a significant pCO_2 drawdown and oversaturated DO due to strong phytoplankton production supported by high nutrients from the river (Dai et al., 2008). Figure 5a generally reflected a combination of photosynthesis-respiration, water mixing and other physical processes in the PRE (see Sect. 4).

In the nearshore area of Transect B, associated with a coastal upwelling system (Figs. 1, 2b), pCO_2 and DO saturation had a significant negative correlation (Fig. 5b, slope=-164μatm, r=-0.88). Similar slope was also found in the nearshore regions of Transect D and west side of Transect E (close to the Transect D) (Fig. 5d), where another upwelling system was also located (Figs. 1, 2e). In contrast, in the offshore area of Transect B where an estuarine plume existed, pCO_2 and DO saturation distinctly followed another negative correlation (slope=$-1465\ \mu$atm, r=-0.94, Fig. 5b). In the offshore areas of Transects A, C, and D, no correlation could be developed between pCO_2 and DO saturation (Fig. 5).

In summary, we observed three pCO_2-DO relationships, which implied different biogeochemical processes in different regions of the northern SCS. Below we will discuss them in details.

4 Discussion

In light of the effects of heating/cooling on both the pCO_2 and DO saturation (4.23%°C^{-1} vs. 1.60%°C^{-1}, the latter was calculated based on our real dataset), we normalized sea surface pCO_2 to the mean SST (29°C) following the approach of Zhai et al. (2005a). And then we examined the relationship between the temperature normalized pCO_2 (NpCO_2 hereafter) and EO_2 (Fig. 6).

4.1 Linking DO to pCO_2 in the upwelling induced highly productive areas based on Redfield ratio and Revelle factor

In highly productive areas, net metabolic processes (i.e. a combination of primary production and respiration) typically cause negatively correlated variations of dissolved inorganic carbon (DIC) and DO. However, the relationship between pCO_2 and DO is more complicated because pCO_2 is buffered by the marine carbonate system characterized by the Revelle factor. In contrast DO is not associated with any buffer system. The Revelle factor is defined as the ratio of fractional change in seawater pCO_2 to the fractional change in total DIC after re-equilibration, i.e. $[\partial pCO_2/pCO_2]/[\partial \mathrm{DIC}/\mathrm{DIC}]$ at a given temperature, salinity and alkalinity (Revelle and Suess, 1957; Sundquist et al., 1979). In the oligotrophic basin area of the northern SCS, the surface-water Revelle factor has been estimated to be about 9 (Tseng et al., 2007). Based on the conservative mixing line of the carbonate system in the northern SCS, as summarized in Dai et al. (2008), the maximum possible Revelle factor value at salinity of ≈30 could be estimated as 11. Air-equilibrated surface DIC (1900 μmol kg^{-1}) in the offshore regions was taken from Tseng et al. (2007). The air-equilibrated pCO_2 was equivalent to the mean value of field measured atmospheric pCO_2.

In the following discussion, we first converted the EO_2 value into DIC change based on the classic Redfield Ratio, and then used the Revelle factor to convert this DIC change into pCO_2 change at the given temperature, thereby linking EO_2 to pCO_2 change in order to characterize the net metabolic processes. Therefore, several possible photosynthesis-respiration-dominant lines of NpCO_2 vs. EO_2 at different Revelle factors of 9 and 11 were plotted in Fig. 6a according to Eq. (2):

$$\begin{aligned}\delta \mathrm{N}pCO_2 &= \mathrm{RF}\times\left(\mathrm{N}pCO_2^0/\mathrm{DIC}^0\right)\times\delta\mathrm{DIC} \\ &= \mathrm{RF}\times\left(\mathrm{N}pCO_2^0/\mathrm{DIC}^0\right)\times(-\delta EO_2)\times(106/138)\end{aligned} \quad (2)$$

where prefix δ means a differential change, superscript 0 the air-equilibrated value, RF the Revelle factor, 106/138 the classic Redfield ratio between carbon and O_2 changes.

Both the datasets from the two coastal upwelling systems (nearshore areas of Transects B and D, together with west part of the Transect E) followed the seawater Redfield lines (Fig. 6a), although some NpCO_2 data were higher than the air-equilibrated level in the central areas of the two upwelling systems. If considering the temperature effect again, based on Eq. (2) we could also expect the slope of the photosynthesis-respiration-dominant pCO_2 vs. DO plot as $-\mathrm{RF}\times(\mathrm{N}pCO_2^0/\mathrm{DIC}^0)\times(106/138)/(4.23/1.60) = -0.5$ or

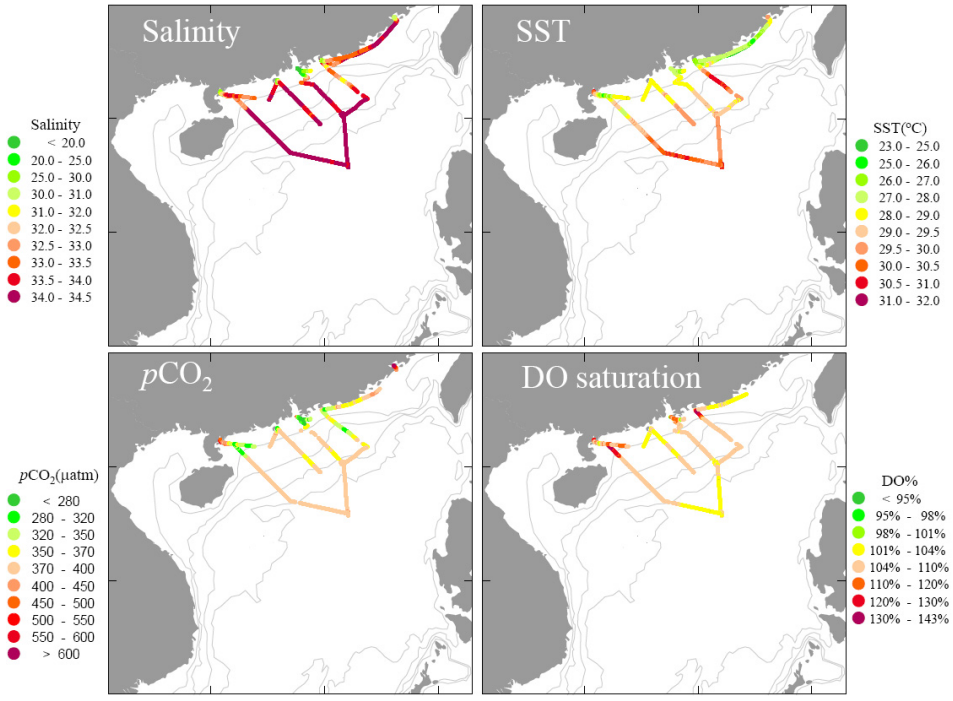

Fig. 4. Geographic distributions of sea surface salinity, temperature, pCO_2 and DO saturation along surveying tracks under study in July 2004.

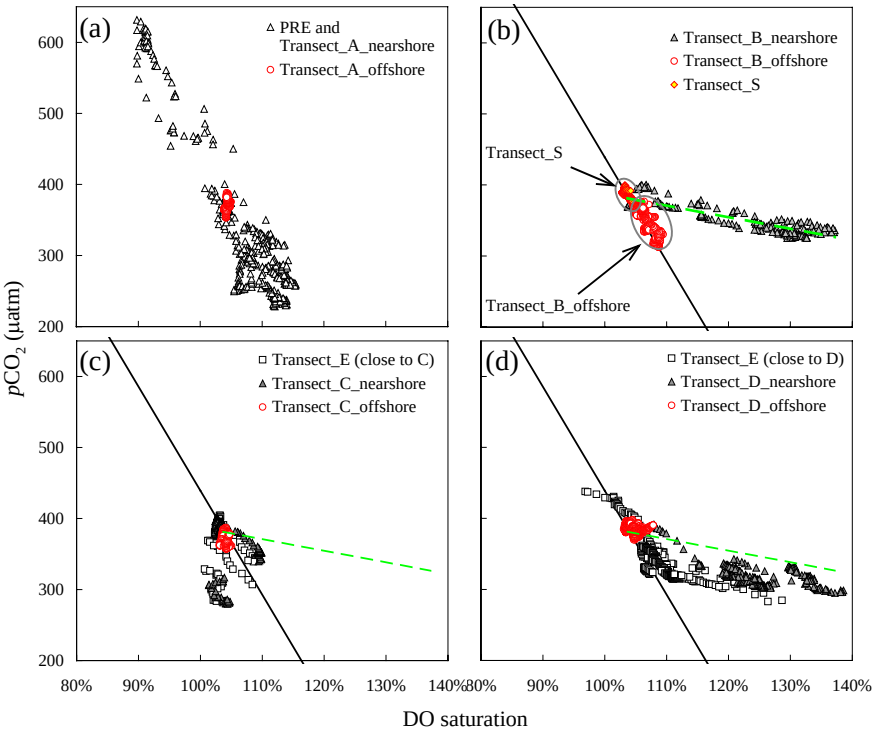

Fig. 5. Relationship between surface pCO_2 and DO saturation along different transects. The two regression lines, fitted by minimizing the sum of the squares of the y-offsets, are: in the nearshore area in Transect B–y=−164 x+552 (R^2=0.79, dashed lines) and the offshore area in Transect B–y=−1465 x+1904 (R^2=0.88, solid lines).

$-0.6\,\mu$atm$-pCO_2$ (μmol-O_2 kg^{-1})$^{-1}$, where 4.23/1.60 is the typical ratio of temperature effects on pCO_2 and DO saturation (see discussion above). Therefore the slope of photosynthesis-respiration-dominant pCO_2 vs. DO% plot should be between -135 and $-160\,\mu$atm/%DO, given the DO saturation of 135% in nearshore areas in Transects B and D (Fig. 2b) and the air-saturated DO value of $200\,\mu$mol O_2 kg^{-1} in summer in the northern SCS. This range was roughly consistent with the field-measured pCO_2 vs. DO saturation slope of $-164\,\mu$atm/%DO in these areas (Fig. 5). This suggested that both pCO_2 and DO were mainly driven by biological photosynthesis and respiration in the upwelling-influenced nearshore regions, except in the upwelling center where deep water of high pCO_2 was still observable. Another piece of evidence pointing to the fact that photosynthesis-respiration dominated the upwelling-influenced nearshore region was derived from the surface chl-*a* (Fig. 1; Huang et al., 2008). Most significantly, high chl-*a* values of $>2\,\mu$g L^{-1} were observed at two stations in and around the coastal area of Transect B (Fig. 1), which implied biological perturbations of both DIC and DO.

4.2 Influence of air-sea exchange on pCO_2-DO relationship in offshore regions

Away from the upwelling-influenced regions, however, the relationship of NpCO_2 – EO_2 was markedly different from that shown in Fig. 6a. In the offshore area of Transect B, although NpCO_2 was still significantly correlated with EO_2 (Fig. 6b), the slope was much steeper than in the upwelling influenced nearshore waters. This suggested that such a relationship was not mainly derived from on site biological activity, rather it was modulated by a combination of biological and physical processes during the long-distance mixing with offshore waters.

It is important to recognize that air-sea re-equilibration of CO_2 is slower than DO due to the chemical buffering capacity of the marine carbonate system (DeGrandpre et al., 1997, 1998; Carrillo et al., 2004). Therefore, we cannot directly predict DIC change from O_2 change during the long-distance transportation and mixing.

Based on the classic stagnant film model, the flux of gases between the atmosphere and water can be estimated by an empirical boundary-layer model for gas exchange: Flux=$D_{gas}/z\times\Delta C_{gas}$, where D_{gas} is the molecular diffusion coefficient, z the empirical thickness of a hypothetical stagnant boundary layer, ΔC_{gas} the concentration deficit or overstock in water surface. Thus we must firstly establish an empirical gas exchange ratio (ER) of ΔC_{O_2} (i.e. EO_2) to ΔC_{CO_2} (free CO_2 deficit, $\Delta[CO_2^*]$ hereafter, estimated from air-sea pCO_2 difference at SST and Henry's law constant of CO_2).

At the lowest seawater pCO_2 site in the offshore area of Transect B, $\Delta[CO_2^*]$ could be estimated as $1.2\,\mu$mol kg^{-1} based on air pCO_2 of $358\,\mu$atm and seawater pCO_2 of $313\,\mu$atm at SST of 30.7°C and salinity of 31.7 (Fig. 2b), while EO_2 was observed as $12\,\mu$mol kg^{-1} (Fig. 6b). Therefore the ratio of EO_2 to $\Delta[CO_2^*]$ was estimated as 10.7. This was nearly the lowest disequilibrium ratio in this region. Based on our field-measured dataset in this region, the ratio of EO_2 to $\Delta[CO_2^*]$ varied between 9.7 and 22. This ratio, further based on the diffusion coefficient ratio of O_2 to CO_2 ($\sim$1.2, Broecker and Peng 1982), would lead to the lowest air-water exchange ratio of O_2 to CO_2 of (9.7 $\times$1.2):1 = 12:1 and the highest ratio of (22$\times$1.2):1 = 26:1 in the offshore area of our Transect B.

Similar to Eq. (2), Eq. (3) gave the quantitative expression of NpCO_2 vs. DO at a given ER of O_2 to DIC:

$$\begin{aligned}\delta \mathrm{N}pCO_2 &= \mathrm{RF}\times(\mathrm{N}pCO_2^0/\mathrm{DIC}^0)\times\delta\mathrm{DIC}\\ &= \mathrm{RF}\times(\mathrm{N}pCO_2^0/\mathrm{DIC}^0)\times(-\delta EO_2)\times(1/\mathrm{ER})\end{aligned} \quad (3)$$

Based on the above ER factors and Eq. (3), assuming a RF of 10, we could estimate the steepest air-sea exchange induced slope of NpCO_2-EO_2 plot in the offshore area of Transect B by $\delta \mathrm{N}pCO_2/\delta EO_2 = -\mathrm{RF}\times \mathrm{N}pCO_2^\circ/\mathrm{DIC}^\circ \times (1/\mathrm{ER}) = -10\times(360/1900)\times(1/12) = -0.15\,\mu\mathrm{atm} - pCO_2\left(\mu\mathrm{mol}-\mathrm{O_2kg^{-1}}\right)^{-1}$, or $-41\,\mu$atm for the slope of pCO_2-DO% plot, given the maximum DO saturation of 138% in nearshore areas in Transects B and D (Fig. 2b) and the air-saturated DO value of $200\,\mu$mol O_2 kg^{-1} in summer in the northern SCS. This suggested that an integration of the on-site photosynthesis-respiration prior to our cruise and the air – sea exchange during later buoyant transportation might have resulted in the unique pattern of the pCO_2-DO relationship in the offshore region of our Transect B (Fig. 6b). The relatively homogeneous but lower chl-*a* concentration in this region ($\sim$0.5 μg L^{-1}, Fig. 1), compared with the high chl-*a* values of 3–5 μg L^{-1} in the nearshore area of Transect A, the source area of the offshore low-salinity region of Transect B, supported such a pattern, assuming we can use chl-*a* to make implications about on site biological perturbations of both DIC and DO. Similar patterns have been reported in the outer Changjiang (Yangtze River) Estuary, East China Sea (Zhai and Dai, 2009).

In order to justify the above proposed effect of air-sea exchanges on the pCO_2-DO relationship, we adopted the approach by Carrillo et al. (2004) and modelled the air-sea exchange induced re-equilibration of both O_2 and CO_2 after a Redfield-based disturbance. Modelled air-sea gas fluxes were calculated based on the revised gas transfer coefficient equation of Wanninkhof (1992) by Sweeney et al. (2007), i.e. k(cm h^{-1}) =$0.27\times u^2\times$(Sc/Sc@20°C)$^{-0.5}$, where k is the gas transfer velocity, u a constant wind speed of 5 m s^{-1}, Sc the Schmidt number in seawater, Sc@20°C the Sc value in seawater at 20°C, i.e. 660 for CO_2 and 590 for O_2. During the modeling, temperature and salinity were set to 29°C and 32, respectively. At each time step, air-sea exchange induced changes of DIC and DO were calculated based on a constant upper mixed layer depth of 20 m. Sea surface

pCO_2 was then calculated from DIC using a Revelle factor of 10 (see discussion above). The air-sea flux was calculated for every time step of 1 day. Fig. 5b presented those modelled NpCO_2-EO_2 relationships in the 5th, 10th and 15th days. This modelling exercise clearly showed that, a combination of photosynthesis-respiration processes and air-sea exchanges of approximate 15 days could result in the unique NpCO_2-EO_2 relationship in offshore waters along our Transect B. This time scale was reasonable if we considered relevant processes of the mid-May heavy rainfall (China MWR-BH, 2005) leading to an estuarine plume (~10 days), nutrients associated the plume inducing phytoplankton production (~10 days, Dai et al., 2008), the bloom decaying (sustaining 15–20 days), and CO_2 and O_2 re-equilibrating with air (10–30 days through to our surveying). Carrillo et al. (2004) also found that, sea surface O_2 approached atmospheric equilibrium in approximate 30 days, while pCO_2 only changed by approximate 12% during the same time span.

Here we need to discuss the uncertainty of our EO_2 definition Eq. (1). Although the bubble effect of 2.5% supersaturation we adopted from Broecker and Peng (1982) and Stigebrandt (1991) should be reasonable to be applied to the study area, this supersaturation might be subject to variations given the heterogeneity in terms of surface turbulence wave field. Consequently, using a fixed supersaturation rate to characterize the bubble effect could result in uncertainties. For example, data points of NpCO_2-EO_2 in offshore areas and the PRE showed a horizontal shift of $<5\,\mu mol\,O_2\,kg^{-1}$ from the supposed air-equilibrium mark (Fig. 6b, c). However, such uncertainties ($<5\,\mu mol\,O_2\,kg^{-1}$) should be minor in nearshore areas and the PRE, given the fact that ranges of calculated EO_2 spatial variations were as high as $80\,\mu mol\,kg^{-1}$ in nearshore areas (Fig. 6a) and $50\,\mu mol\,kg^{-1}$ in the PRE (Fig. 6c). In the offshore estuarine plume area of Transect B, the largest uncertainty of Eq. (1) might amount to a half of the range of EO_2 variation (Fig. 6b). Therefore the above-estimated time delay should actually range between 10 and 30 days, due solely to this bubble effect uncertainty.

In most other offshore areas than the estuarine plume area of Transect B, however, the NpCO_2 or pCO_2 varied independently from EO_2 or DO (Figs. 5, 6b). This low photosynthesis-respiration signal between pCO_2 and DO in the offshore waters was consistent with the low chl-*a* of $<0.3\,\mu g\,L^{-1}$ therein (Fig. 1) and represented the low regional productivity. Just prior to our cruise, both primary and new production were measured in the offshore region under study (Chen and Chen, 2006). Primary production (PP) was $31\pm12\,mmol\,C\,m^{-2}\,d^{-1}$ in the basin and $72\pm22\,mmol\,C\,m^{-2}\,d^{-1}$ on the shelf (Chen and Chen, 2006). Both were among the lowest of the world's oceans. If we used the above average photosynthetic rate and assumed an euphotic layer of 100 m, the overall impact of biological activity on the surface CO_2 system might be no more than $0.72\,\mu mol\,C\,L^{-1}\,d^{-1}$ (72/100=0.72 $mmol\,C\,m^{-3}\,d^{-1}$),

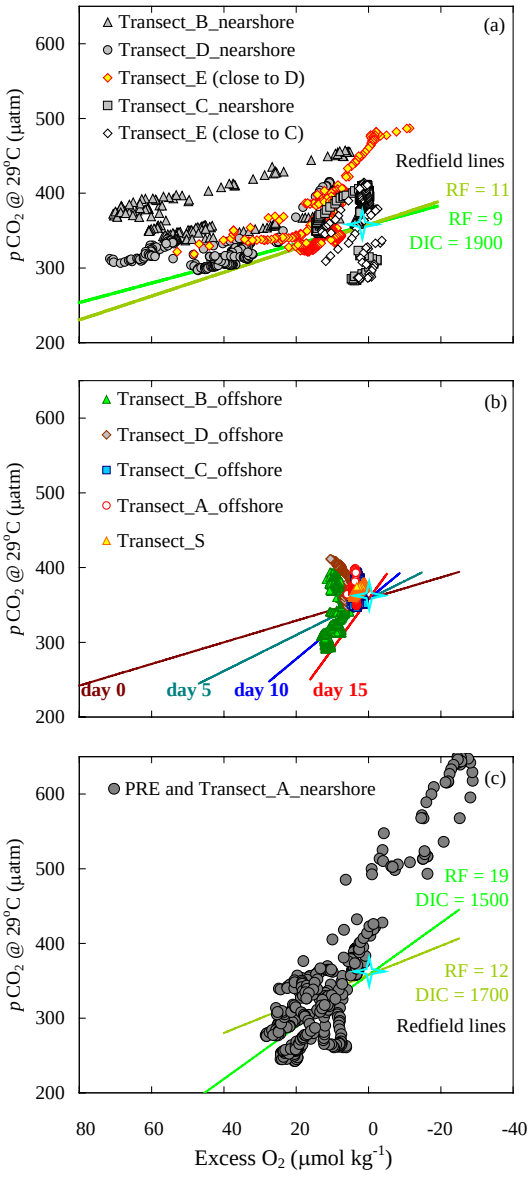

Fig. 6. Temperature normalized pCO_2 (pCO_2 @29°C) vs. excess O_2. The cross star shows the mean atmospheric pCO_2 and the zero excess O_2. In penal **(a)**, the two solid lines show Redfield behavior of pCO_2 @29°C vs. excess O_2 at different Revelle factors (RF) of 9 and 11 in the northern South China Sea (assuming the dissolved inorganic carbon concentration as $1900\,\mu mol\,kg^{-1}$, and ignoring air-sea exchanges). In panel **(b)**, the four solid lines show the single effect of air-sea exchanges on relationship of pCO_2 @29°C vs. excess O_2 as a function of transportation days after the on site primary production/respiration, given a salinity of 32, a temperature of 29°C, the RF of 10, the upper mixed layer depth of 20 m and a steady wind speed of $5\,m\,s^{-1}$, based on gas transfer coefficient equation of Wanninkhof (1992) revised by Sweeney et al. (2007). In panel **(c)**, the two solid lines show Redfield behavior of pCO_2 @29°C vs. excess O_2 at different RF in the Pearl River estuary. Note that the estimated excess O_2 may be subject to uncertainties (see text for details).

which would be equivalent to $<1.5\,\mu$atm of pCO_2 change per day, converted from a Revelle factor of 10 as discussed above or DO $<1.0\,\mu$mol L^{-1} change per day based on the classic Redfield ratio. If we took into consideration the respiration, the net effect of the biological metabolism might be close to zero. Indeed, the new production was determined to be only ~7% (shelf) to 30% (basin) of the PP, indicating that the PP was mostly recycled on a daily time scale (Chen and Chen, 2006). Therefore, the net effects of biological activity on both pCO_2 and DO were minor in the outer shelf/slope and basin waters.

4.3 Influence of weak CO_2 buffering capacity in PRE and adjacent nearshore areas

In the PRE, DIC was ~1500 μmol kg^{-1} (Dai et al., 2008) and the Revelle factor varied from 19 to 12 along with salinity increased from 15 to 25, based on the conservative mixing line of the carbonate system, as summarized in Dai et al. (2008). This is apparently caused by higher concentrations of free CO_2 in the estuarine waters than in the offshore water (Zhai et al., 2005a, b).

We could, therefore, model possible photosynthesis-respiration-dominant lines of NpCO_2 vs. EO_2 in the PRE based on the classic Redfield ratio and possible Revelle factor of 12–19 (Fig. 6c). The reasonable agreement between data and predicted values (Fig. 6c) suggested that the drawdown of pCO_2 and enhancement of DO in the PRE were mainly influenced by on site primary production, while air - water gas exchange might also have contributions, with much smaller effects than in the offshore estuarine plume area, apparently due to the shorter residence time there.

The comparison of different NpCO_2-EO_2 relationships between coastal upwelling influenced areas and the PRE (Fig. 6a, c) showed significant effect of the Revelle factor on surface pCO_2 dynamics. Although pCO_2-DO relationships in nearshore areas of Transects A and B were both dominated by photosynthesis/respiration, different Revelle factors resulted in different pCO_2-DO slopes in the two waters (Fig. 5a, b).

5 Conclusions

In this study, we elucidated the effect of photosynthesis/respiration and air-water exchange on the changes in the coupling of pCO_2 and DO in a spectrum of coastal settings in the northern SCS. In the coastal upwelling influenced areas, both properties were mainly controlled by on site net community metabolic processes. In the estuarine plume influenced regions, the pCO_2-DO relationship was controlled by the integrated effect of previous community metabolic processes and subsequent air-water exchange. Moreover, the chemical buffering of the carbonate system had a significant effect on the relationship.

We must point out that our study was based on a limited data set, and therefore the specific results observed were by no means general. This study, nevertheless, revealed that a combination of high-resolution CO_2 and O_2 measurements could provide valuable information regarding net metabolic status in marine ecosystems under different physical and biogeochemical conditions such as upwelling and water transport time. We have demonstrated a simple procedure in evaluating the community metabolic status based on these surface pCO_2 and DO measurements. This approach may have applicability in many other coastal systems with a large gradient of changes in their physical and biogeochemical conditions.

Acknowledgements. This research was supported by the Natural Science Foundation of China through grants #90711005, #40731160624, #40876040 and #40821063. The manuscript preparation was supported by the National Basic Research Program ("973" Program) of China (#2009CB421201, the CHOICE-C project) and by internal fund of State Key Laboratory of Marine Environmental Science (Xiamen University). We thank Wuqi Ruan, Pinghe Cai, and Fan Zhang along with the crew of R/V Yanping II for their much help during the sampling cruise, Baoshan Chen and Zhaozhang Chen for their assistance in the data collection and Justin Hartmann for his assistance with English. Finally, we are grateful to Fiz F. Pérez, David Hydes, Joe Salisbury and an anonymous reviewer for their constructive comments and suggestion on the manuscript.

Edited by: A. V. Borges

References

Álvarez, M., Ríos, A. F., and Rosón, G.: Spatio-temporal variability of air-sea fluxes of carbon dioxide and oxygen in the Bransfield and Gerlache Straits during austral summer 1995–96, Deep-Sea Res. Pt. II, 49, 643–662, 2002.

Benson, B. B. and Krause, D.: The concentration and isotopic fractionation of oxygen dissolved in fresh water and seawater in equilibrium with the atmosphere, Limnol. Oceanogr., 29, 620–632, 1984.

Borges, A. V., Delille, B., and Frankignoulle, M.: Budgeting sinks and sources of CO_2 in the coastal ocean: Diversity of ecosystems counts, Geophys. Res. Lett., 32, L14601, doi:10.1029/2005GL023053, 2005.

Borges, A. V. and Frankignoulle, M.: Short-term variations of the partial pressure of CO_2 in surface waters of the Galician upwelling system, Prog. Oceanogr., 51, 283–302, 2001.

Broecker, W. S. and Peng, T. H.: Tracers in the sea, Eldigio Press, Palisades, NY, 690 pp., 1982.

Carrillo, C. J., Smith, R. C., and Karl, D. M.: Processes regulating oxygen and carbon dioxide in surface waters west of the Antarctic Peninsula, Mar. Chem., 84, 161–179, 2004.

Cai, W.-J., Dai, M. H., and Wang, Y. C.: Air-sea exchange of carbon dioxide in ocean margins: a province-based synthesis, Geophys. Res. Lett., 33, L12603, doi:10.1029/2006GL026219, 2006.

Cai, W.-J. and Dai, M. H.: Comment on "Enhanced open ocean storage of CO_2 from shelf sea pumping", Science, 306, p. 1477, 2004.

Chen, C.-T. A. and Borges, A. V.: Reconciling opposing views on carbon cycling in the coastal ocean: continental shelves as sinks and nearshore ecosystems as sources of atmospheric CO_2, Deep Sea Res. II, 56, 578–590, 2009.

Chen, Y.-L. L. and Chen, H.-Y.: Seasonal dynamics of primary and new production in the northern South China Sea: the significance of river discharge and nutrient advection, Deep-Sea Res. I, 53, 971–986, 2006.

China MWR-BH (Bureau of Hydrology, Ministry of Water Resources, China): Hydrological Information Annual Report 2004, China Water Power Press, Beijing, China, 104 pp., 2005 (in Chinese).

Dai, M. H., Zhai, W. D., Cai, W. J., Callahan, J., Huang, B. Q., Shang, S. L., Huang, T., Li, X. L., Lu, Z. M., Chen, W. F., and Chen, Z. Z.: Effects of an estuarine plume-associated bloom on the carbonate system in the lower reaches of the Pearl River estuary and the coastal zone of the northern South China Sea, Cont. Shelf Res., 28, 1416–1423, 2008.

DeGrandpre, M. D., Hammar, T. R., and Wirick, C. D.: Short-term pCO_2 and O_2 dynamics in California coastal waters, Deep-Sea Res. II, 45, 1557–1575, 1998.

DeGrandpre, M. D., Hammar, T. R., Wallace, D. W. R., and Wrick, C. D.: Simultaneous mooring-based measurements of seawater CO_2 and O_2 off Cape Hatteras, North Carolina, Limnol. Oceanogr., 42, 21–28, 1997.

Guéguen, C. and Tortell, P. D.: High-resolution measurement of Southern Ocean CO_2 and O_2/Ar by membrane inlet mass spectrometry, Mar. Chem., 108, 184–194, 2008.

Gago, J., Gilcoto, M., Pérez, F. F., and Ríos, A. F.: Short-term variability of fCO_2 in seawater and air-sea CO_2 fluxes in a coastal upwelling system (Ría de Vigo, NW Spain), Mar. Chem., 80, 247–264, 2003.

Gan, J. P., Li, L., Wang, D. X., and Guo, X. G.: Interaction of a river plume with coastal upwelling in the northern South China Sea, Cont. Shelf Res., 29, 728–740, 2009.

Han, W. Y.: Marine chemistry in the South China Sea, Science Press, Beijing, China, 289 pp., 1998 (in Chinese).

Hu, J. Y., Kawamura, H., Hong, H. S., and Qi, Y. Q.: A review on the currents in the South China Sea: Seasonal circulation, South China Sea Warm Current and Kuroshio intrusion, J. Oceanogr., 56, 607–624, 2000.

Huang, B. Q., Lan, W. L., Cao, Z. R., Dai, M. H., Huang, L. F., Jiao, N. Z., and Hong, H. S.: Spatial and temporal distribution of nanoflagellates in the northern South China Sea, Hydrobiologia, 605, 143–157, 2008.

Jing, Z. Y., Qi, Y. Q., Hua, Z. L., and Zhang, H.: Numerical study on the summer upwelling system in the northern continental shelf of the South China Sea, Cont. Shelf Res., 29, 467–478, 2009.

Körtzinger, A., Send, U., Wallace, D. W. R., Karstensen, J., and DeGrandpre, M.: Seasonal cycle of O_2 and pCO_2 in the central Labrador Sea: Atmospheric, biological, and physical implications, Global Biogeochem. Cy., 22, GB1014, doi:10.1029/2007GB003029, 2008.

Kuss, J., Roeder, W., Wlost, K.-P., and DeGrandpre, M. D.: Time-series of surface water CO_2 and oxygen measurements on a platform in the central Arkona Sea (Baltic Sea): seasonality of uptake and release, Mar. Chem., 101, 220–232, 2006.

Revelle, R. and Suess, H. E.: Carbon dioxide exchange between atmosphere and ocean and the question of an increase of atmospheric CO_2 during the past decades, Tellus, 9, 18–27, 1957.

Stigebrandt, A.: Computations of oxygen fluxes through the sea surface and the net production of organic matter with application to the Baltic and adjacent seas, Limnol. Oceanogr., 36, 444–454, 1991.

Sundquist, E. T., Plummer, L. N., and Wigley, T. M. L.: Carbon dioxide in the ocean surface: the homogenous buffer factor, Science, 204, 1203–1205, 1979.

Sweeney, C., Gloor, E., Jacobson, A. R., Key, R. M., McKinley, G., Sarmiento, J. L., and Wanninkhof, R.: Constraining global air-sea gas exchange for CO_2 with recent bomb ^{14}C measurements, Global Biogeochem. Cy., 21, GB2015, doi:10.1029/2006GB002784, 2007.

Takahashi, T., Olafsson, J., Goddard, J. G., Chipman, D. W., and Sutherland, S. C.: Seasonal variation of CO_2 and nutrients in the high-latitude surface ocean: a comparative study, Global Biogeochem. Cy., 7, 843–878, 1993.

Tseng, C. M., Wong, G. T. F., Chou, W. C., Lee, B. S., Sheu, D. D., and Liu, K. K.: Temporal variations in the carbonate system in the upper layer at the SEATS station, Deep-Sea Res. II, 54, 1448–1468, 2007.

Wanninkhof, R.: Relationship between wind speed and gas exchange over the ocean, J. Geophys. Res., 97, 7373–7382, 1992.

Weiss, R. F. and Price, R. A.: Nitrous oxide solubility in water and seawater, Mar. Chem., 8, 347–359, 1980.

Wong, G. T. F., Ku, T.-L., Mulholland, M., Tseng, C.-M., and Wang, D.-P.: The SouthEast Asian Time-series Study (SEATS) and the biogeochemistry of the South China Sea: an overview, Deep-Sea Res. II, 54, 1434–1447, 2007.

Wu, R. S. and Li, L.: A summary of studies on upwelling system in the South China Sea, J. Oceanogr. Taiwan Str., 22, 269–277, 2003 (in Chinese).

Zhai, W. D. and Dai, M. H.: On the seasonal variation of air-sea CO_2 fluxes in the outer Changjiang (Yangtze River) Estuary, East China Sea, Mar. Chem., doi:10.1016/j.marchem.2009.02.008, in press, 2009.

Zhai, W. D, Dai, M. H., Cai, W.-J., Wang, Y. C., and Hong, H. S.: The partial pressure of carbon dioxide and air-sea fluxes in the northern South China Sea in spring, summer and autumn, Mar. Chem., 96, 87–97, 2005a. [Erratum: Mar. Chem., 103, 209, 2007].

Zhai, W. D., Dai, M. H., Cai, W.-J., Wang, Y. C., and Wang, Z. H.: High partial pressure of CO_2 and its maintaining mechanism in a subtropical estuary: the Pearl River estuary, China, Mar. Chem., 93, 21–32, 2005b.